# Performance Evaluation of Stress Absorbing Membrane Interlayers Considering Debonding Effects

Ogundipe Olumide Moses

Civil Engineering Department, Ekiti State University, Ado-Ekiti, Nigeria
P.M.B. 5363, Ado-Ekiti, Ekiti State, Nigeria

momide2002@yahoo.com

***Abstract-*****This study investigates debonding effects on the performance of stress absorbing membrane interlayers (SAMIs) against reflective cracking. This was achieved by carrying out finite element modelling of a typical specimen used for a wheel tracking test. In the modelling, the loads were applied at two points (centre and edge) on the specimen. The predicted results (deflection and strain) were compared with those measured in the laboratory tests. The results showed that the predicted results for the debonding cases matched those measured better than the fully bonded cases. This indicates that the debonding of the interface is expected in a real pavement incorporating SAMIs. Also, the results showed that there was no benefit in using thick SAMI over thin SAMI. It was found that the predicted deflection, strain, and stress increase with increasing temperature.**

***Keywords- Finite Element; Overlay; Debond; Displacement; Strain; Stress***

## I. INTRODUCTION

Rehabilitation of pavements by overlaying a new surfacing material is usually rendered less effective by reflective cracking. Shalaby and Frenchette [1] defined reflective cracking as the premature occurrence of cracks on overlays at positions and orientations that corresponds to locations of cracks in lower pavement layers. Song et al. [2] stated that cracking has occurred in nearly all types of asphalt overlays due to mechanical and environmental loadings. Cracks in pavement allow water to penetrate it, leading to deterioration of the foundation of the pavement structure. Engineers have tried to overcome the problem using different measures. These include thick overlay, overlay mixture modification, overlay reinforcement, stress or strain absorbing interlayer and reinforcing interlayer. It has also been found that the performance of the overlay depends on the bond strength between the interlayer material, existing pavement and overlay. A number of factors affect interface bond [3, 4]. These include construction practice, the materials in contact, amount of tack coat, interface condition, etc.

Scarpas and de Bondt [5] observed in their study using finite element simulations that higher improvement factors can be obtained for stiff reinforcing products by increasing the bond stiffness. Kwon et al. [6] investigated geogrid reinforcement mechanism by varying the shear stiffnesses in the interface elements to specify various levels of interface bonding, i.e. perfect bonding, partial bonding with geogrid, and no geogrid (unreinforced). They performed linear and nonlinear analyses that included isotropic and cross-anisotropic base course characterizations. Their results indicated that the response and eventually, the performance of a typical highway pavement could be enhanced by the inclusion of geogrids. The results of their numerical study also demonstrated the stiffening around the geogrid reinforcement due to increased confinement by the slightly increased modulus properties in the vicinity of the geogrid reinforcement. As observed by Kim and Buttlar [7], the primary benefit of a soft interlayer is to reduce the longitudinal stresses in the overlay caused by wheel load and/or thermal cycling

Ozer et al. [8] studied the influence of interface bonding conditions on the critical strains in hot mix asphalt (HMA) overlaid PCC pavements. They developed a numerical model to gain better understanding of the pavement interface behaviour. They found that HMA bottom tensile strains increased drastically due to excessive tack coat application rate during construction. Their modelling results underscored the importance of tack coat application rate. Also, they showed that the HMA tensile strains can be significantly amplified with less stiff interface properties which correspond to decreasing bonding strength.

In mechanistic analysis, hot-mix asphalt has traditionally being considered to behave in a linear elastic manner. This has some shortcomings for that, in reality, asphalt concrete behaves more like a viscoelastic material. Hot-mix asphalt only behaves as an elastic material at low temperature and high loading frequency, while it behaves like a viscous fluid at high temperature and low loading frequency. At intermediate temperatures and loading frequencies, it behaves like a viscoelastic material that exhibits a significant level of elastic solid stiffness while dissipating energy by frictional resistance as a viscous fluid. Although asphalt behaves more like a viscoelastic material, for simplicity it was considered appropriate to use a linear elastic model for the analysis. As observed by Sousa et al. [9], two major factors are of particular interest in the mechanical analysis of hot-mix asphalt: the material characterization method and its accuracy in reflecting the material resistance to loading; and the accuracy of mechanistic models to predict the pavement performance.

In this study, a finite element analysis was carried out using Abaqus commercial finite element software. The finite element analysis allowed the prediction of displacements and strain in the crack region, which were then compared to the measurements from laboratory tests. Also, the stress in the crack region was predicted in the finite element analysis.

## II. FINITE ELEMENT FORMULATION FOR THE WHEEL TRACKING TEST

The wheel tracking test device with sample in place is shown in Fig. 1. A linear elastic material model was adopted for the study. Therefore, the material properties required for the finite element modelling are the elastic modulus, E and Poisson's ratio, μ. The elastic modulus (stiffness) was determined using the indirect tensile stiffness modulus (ITSM). The stiffness was used directly because the temperatures were the same and wheel loading rate was close to the ITSM loading rate. The mix composition and properties of each of the layers at 10 $^{o}$C, 20 $^{o}$C and 30 $^{o}$C are shown in Tables 1 and 2, respectively. Cracks in an existing pavement have been modelled using different approaches by researchers. Wu and Harvey [10] modelled a crack with empty spaces in the underlying layer; Minhoto et al. [11] in their study of reflective cracking behaviour for traffic and temperature effects modelled cracks using elements without stiffness. Pais and Pereira [12] modelled cracks as a void with a negligible stiffness of 1MPa. In this study, for simplicity, the crack was modelled by assigning a low material stiffness (overstressing) to the elements.

The parameters considered in the modelling include the overlay and stress absorbing membrane interlayer (SAMI) thicknesses, and the test temperature.

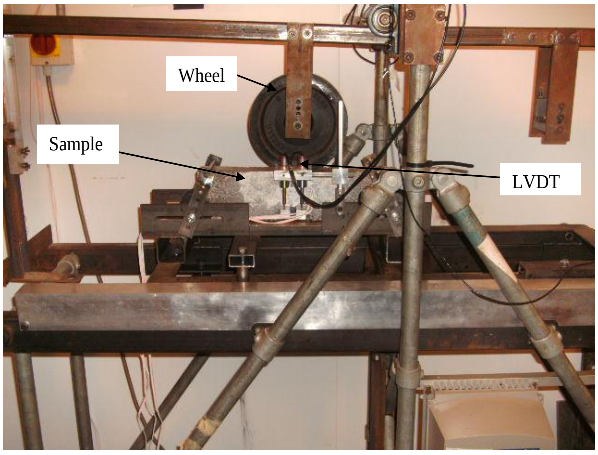


Fig. 1 Wheel tracking device with the sample in place

TABLE 1 MIX COMPOSITIONS FOR THE SAMIS

| Sample type | % by composition of aggregate | % by composition of aggregate | % by composition of aggregate |
|---|---|---|---|
| | **Proprietary SAMI A** | **Proprietary SAMI B** | **Sand asphalt** |
| 0/4 Crushed Rock Fill | 95% | 74.5% | - |
| fine sand | - | 20% | 84% |
| Filler | 5% | 5.5% | 16% |
| Binder type | Polymer modified binder | Polymer modified binder | 160/220 bitumen |
| Binder content | 9 % by mass of total mix | 9.1 % by mass of total mix | 10.3 % by mass of total mix |
| Target air void | 2% | 2% | 5% |

TABLE 2 LAYER PROPERTIES

| Materials | Properties | | |
|---|---|---|---|
| | **E, MPa, (μ) at 10$^{o}$C** | **E, MPa, (μ) at 20$^{o}$C** | **E, MPa, (μ) at 30$^{o}$C** |
| 10 mm AC (40/60) | 10035 (0.25) | 3899 (0.35) | 1098 (0.45) |
| 10 mm AC (10/20) | 15435 (0.25) | 9591 (0.35) | 5008 (0.45) |
| Proprietary SAMI A | 8548 (0.25) | 2725 (0.35) | 635 (0.45) |
| Proprietary SAMI B | 7564 (0.25) | 2444 (0.35) | 510 (0.45) |
| Sand asphalt | 635 (0.25) | 209 (0.35) | 118 (0.45) |
| Crack | 1 (0.35) | | |
| Rubber | 6.45 (0.49) | | |
| Steel | 209000 (0.3) | | |

### *A. Model Geometry and Dimension*

To investigate the performance of the SAMIs, two models were developed: one incorporating SAMIs and the other without SAMIs (Control). The modelling was carried out using commercial finite element software (Abaqus). The model length and width were 404 mm and 50 mm, respectively. The overall model thickness varied with thicknesses of the middle (SAMI) and the surface (overlay) layers. The overall thicknesses considered in the model were 110 mm, 120 mm and 130 mm. The combinations investigated are shown in Table 3. Each combination was investigated at 10°C, 20°C and 30°C for the three SAMIs: Proprietary SAMI A and B and sand asphalt.

TABLE 3 COMBINATIONS (C) INVESTIGATED

| Layer thickness (mm) | C1 | C2 | C3 | C4 | C5 (Control) | C6 (Control) | C7 (Control) |
|---|---|---|---|---|---|---|---|
| **Overlay** | 40 | 40 | 60 | 60 | 60 | 70 | 80 |
| **SAMI** | 20 | 30 | 10 | 20 | - | - | - |
| **Base** | 30 | 30 | 30 | 30 | 30 | 30 | 30 |
| **Rubber** | 10 | 10 | 10 | 10 | 10 | 10 | 10 |
| **Steel** | 10 | 10 | 10 | 10 | 10 | 10 | 10 |
| **Total** | 110 | 120 | 120 | 130 | 110 | 120 | 130 |

A 3-dimensional analysis was carried out allowing the load to be placed across the entire beam width of 50 mm as was the case for the laboratory study. All the layers were simulated using an 8-node linear brick, reduced integration element (C3D8R) – a first order isoparametric element. The C3D8R elements have only one integration point, thereby reducing the computational time without any great effect on the result accuracy. The reduced integration means that an integration scheme having one order less than the full scheme was used to integrate the element internal forces and stiffness [13]. Typical 3-dimensional structural model for the wheel tacking test for specimen with 10 mm - SAMI and 60 mm - overlay is shown in Fig. 2, while typical control model (no SAMI) with 60 mm - overlay is shown in Fig. 3. Crack (overstressed part) in the existing pavement was modelled by assigning a low material stiffness to the elements (see Table 2).

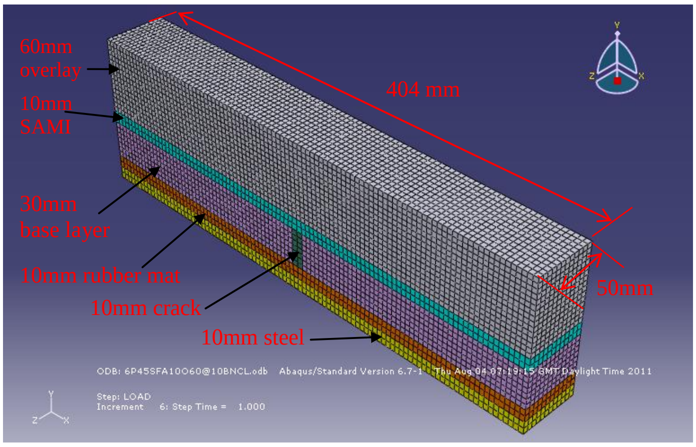


Fig. 2 A typical model with 10 mm - SAMI and 60 mm - overlay

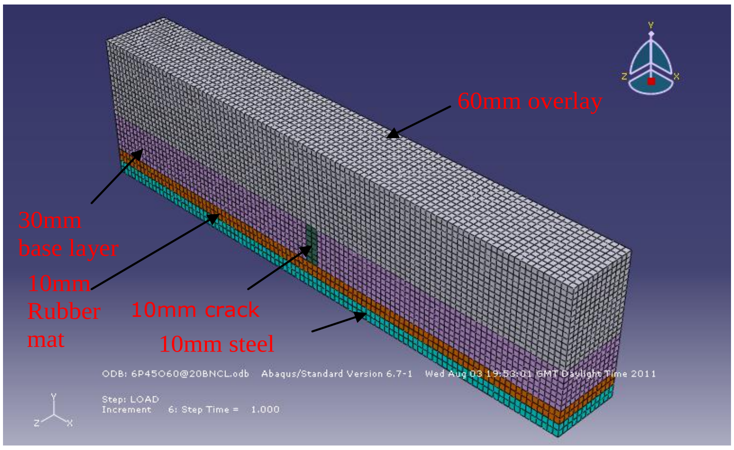


Fig. 3 A typical model (control) 60 mm - overlay

## B. *Loading and Boundary Conditions*

A distributed load of 2.4 kN (1.1MPa) was used in the modelling. It was placed on the whole width (50 mm) of the beam over a length of 45 mm. The load was placed at two different locations on the specimen: 90 mm away from the centre of the crack, termed 'edge load', and directly above the simulated crack, termed 'centre load', as shown in Figs. 4 and 5, respectively and they were modelled separately. Only one side of the model was considered because of symmetry. The model support was simulated by applying a fixed boundary condition to the steel base. The tests simulated pavement continuity by clamping; the model simulated clamping using fixed boundaries. The fixed boundary condition (encastre) constrains the model movement, i.e. the displacement and rotation in x, y and z directions.

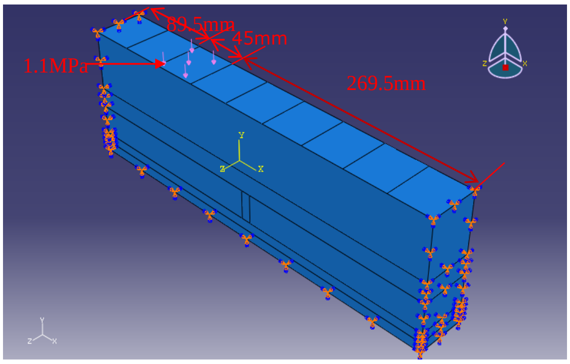


Fig. 4 A typical model assembly with edge load and boundary conditions

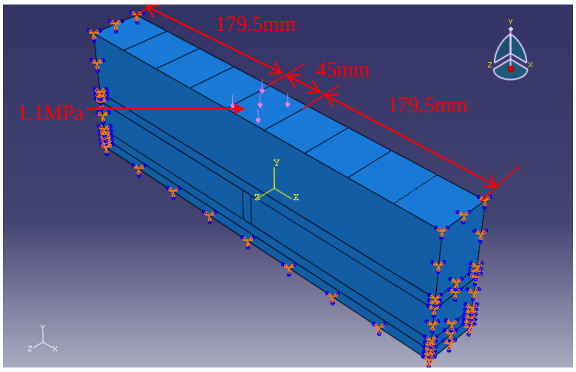


Fig. 5 A typical model assembly with centre loading and boundary conditions

### C. Contact Modelling

Two cases were investigated for the interaction between the layers: overlay-SAMI, SAMI-base, base-rubber and rubber-steel interfaces. The first assumed a full bond condition (compatibility of stresses and strains). The second case assumed a friction-type contact (slip) between the SAMI and the base layers, i.e. the layer interface was allowed to separate (debond), while other interfaces were assumed to be fully bonded. The friction-type contact was achieved by using the penalty contact method. Finite sliding that allows arbitrary motion of the surfaces and the surface - to - surface discretization method were selected in Abaqus CAE. A friction coefficient of 0.7 was used and the default slip tolerance of 0.005 mm specified by Abaqus was used. The values were chosen as trials showed that they could simulate the debonding condition.

## III. RESULTS AND DISCUSSION

The results of the models were obtained at 4 mm above the crack top, the bottom of the overlay and at 20 mm from the bottom of the overlay. For the specimens with 10 mm -, 20 mm - and 30 mm - SAMIs, 20 mm from the bottom of the overlay is equivalent to 30 mm, 40 mm and 50 mm from the bottom of the overlay in their respective control specimens. The specimen references are shown in Table 4.

TABLE 4 SPECIMEN REFERENCES

| Specimens name | Specimens references |
|---|---|
| 60 mm - overlay (Control) | O60 |
| 20 mm - thick sand asphalt with 40 mm - overlay | SA20O40 |
| 20 mm - thick Proprietary SAMI A with 40 mm - overlay | PA20O40 |
| 20 mm - thick Proprietary SAMI B with 40 mm - overlay | PB20O40 |
| 70 mm - overlay (Control) | O70 |
| 30 mm - thick sand asphalt with 40 mm - overlay | SA30O40 |
| 30 mm - thick Proprietary SAMI A with 40 mm - overlay | PA30O40 |
| 30 mm - thick Proprietary SAMI B with 40 mm - overlay | PB30O40 |
| 10 mm - thick sand asphalt with 60 mm - overlay | SA10O60 |
| 10 mm - thick Proprietary SAMI A with 60 mm - overlay | PA10O60 |
| 10 mm - thick Proprietary SAMI B with 60 mm - overlay | PB10O60 |
| 80 mm - overlay (Control) | O80 |
| 20 mm - thick sand asphalt with 60 mm - overlay | SA20O60 |
| 20 mm - thick Proprietary SAMI A with 60 mm - overlay | PA20O60 |
| 20 mm - thick Proprietary SAMI B with 60 mm - overlay | PB20O60 |

*1) Displacement*

The absolute displacement was recorded when the load was at the centre. The measured and predicted absolute displacements at 10 °C, 20 °C and 30 °C are shown in Fig. 6. It can be seen from the figure that there were more absolute displacements in the specimens with SAMIs than the control sections without SAMIs. As observed in the wheel tracking test [14], the results showed that the specimen with smaller SAMI thickness had less displacement than those with greater thickness. Also, it can be seen that the absolute displacements of the specimens increased with temperature. The figure shows that greater displacements were predicted in the debond cases than the full bond cases. The finite element analysis showed that the predicted absolute displacements were more or less the same as the measured values. The debond cases matched the measured value better than those that were fully bonded. The difference between the measured and predicted measurements for the debond cases could be attributed to the modulus of elasticity used in the modeling. They were determined from the indirect tensile stiffness modulus (ITSM) test in the laboratory. The values were used directly as the loadings were believed to be almost the same. However, in the real sense, this might not be correct and may account for the difference observed. Also, higher deflections were predicted in models with thicker SAMIs.

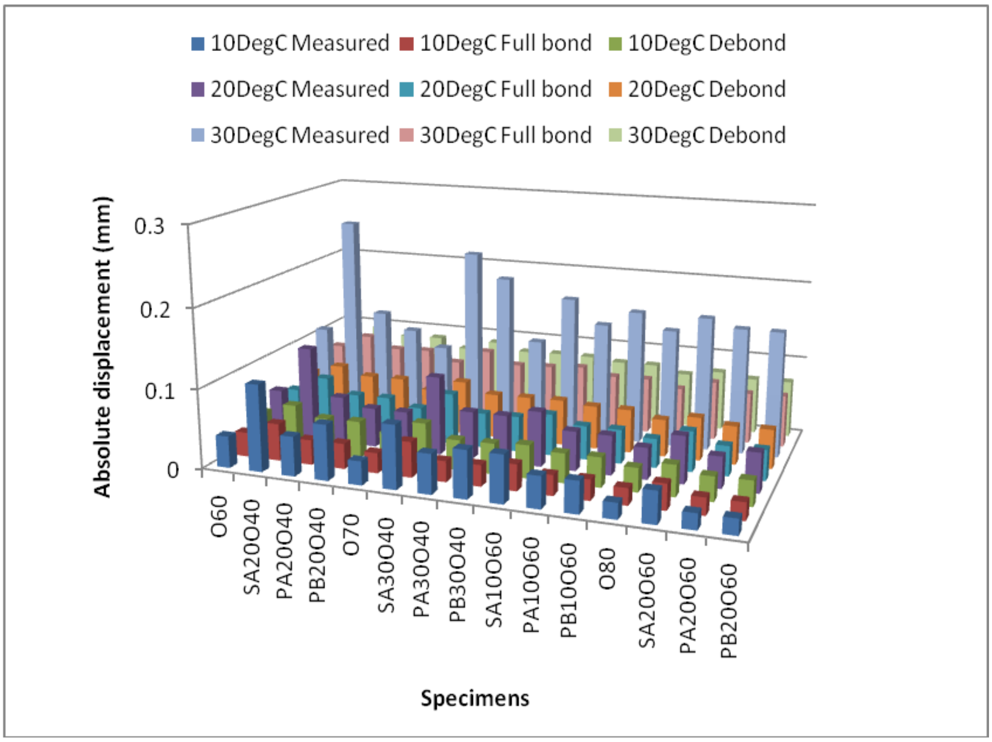


Fig. 6 Absolute displacement at 10 °C, 20 °C and 30 °C (DegC)

*2) Strain*

The strain (measured and predicted) was obtained as the difference in values when the load was placed at the centre directly above the crack top and at the edge (90mm from the centre). The measured and predicted strains at 4mm above the crack top at 10 °C, 20 °C and 30 °C are shown in Fig. 7. It shows that at 10 °C and 20 °C, the measured and predicted tensile strains at 4mm above the crack top in the specimens with SAMIs are greater than strains in the control specimens with no SAMIs for both the full bond and debond conditions, except for the specimens with sand asphalt as SAMI. The use of very soft interlayers (SAMIs) increases deflection of the pavement. This in turn results in high strain concentration around the crack. The figure indicates that at 30 °C for the full bond cases less strain was predicted at 4 mm above the crack top in the specimens with SAMIs than the control specimens without SAMI with the exception of the specimens with sand asphalt, which were in compression, while for the debond cases greater strain was predicted in the specimens with SAMIs than those without SAMI.

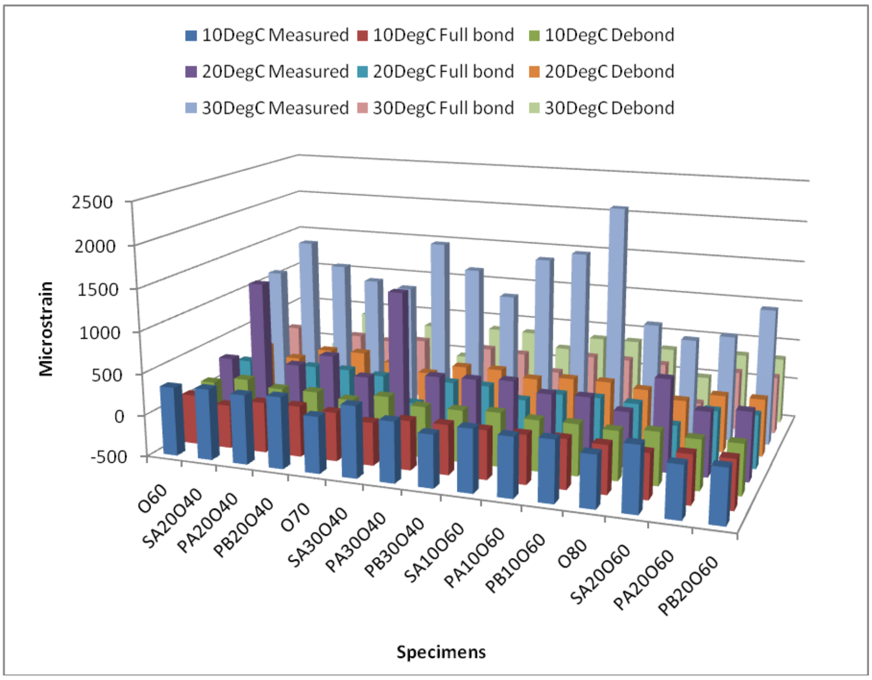


Fig. 7 Strain at 4 mm above the crack top at 10 °C, 20 °C and 30 °C (DegC)

Fig. 8 shows the predicted strain at the bottom of the overlay for both control specimens and those with SAMIs (full bond and the debond cases) at 10 °C, 20 °C and 30 °C (DegC). It can be seen from the figure that the strains at the bottom of the overlay were smaller in the specimens with SAMIs than those without SAMIs. Also, the strains were smaller in specimens with lower SAMIs thickness. Fig. 9 shows the strain (measured and predicted) at 20 mm from the bottom of the overlay at 10 °C, 20 °C and 30 °C (DegC). It indicates that for the specimens with 10 mm - SAMI and 20 mm - SAMI and 60 mm - overlay, smaller strains were measured and predicted in specimens with SAMIs than in those without SAMIs for SAMIs A and B, while the specimens with sand asphalt as SAMI had greater strain than the control.

Fig. 9 shows that at 30 °C the results were mixed. This is probably due to the high load magnitude and temperature. As observed in the laboratory test, the test carried out using a reduced load of 1.35 kN (0.6MPa) at 30 °C showed clearly the crack resistance of SAMI against reflective cracking [14]. Generally, it can be seen from the measured and predicted strains at 20 mm from the bottom of the overlay that, although high strain concentration exists around the crack region in the specimens with SAMIs, they were able to isolate the overlay from the strain concentration. This shows the crack resistance potential of the proprietary SAMIs A and B. Also, it can be seen from the results that greater strains were predicted in the debond cases than the full bond cases.

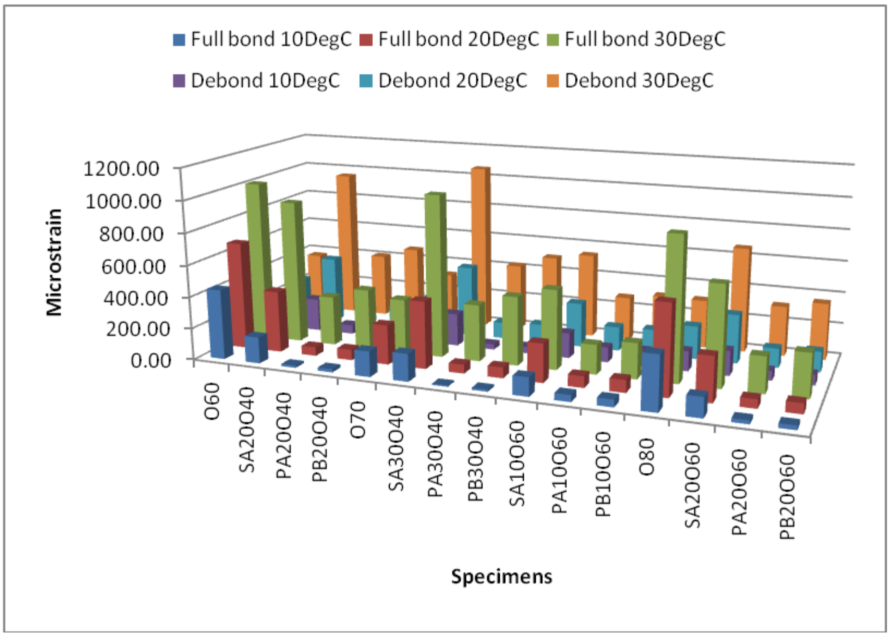


Fig. 8 Strain at the bottom of the overlay at 10 °C, 20 °C and 30 °C (DegC) (full bond and Debond)

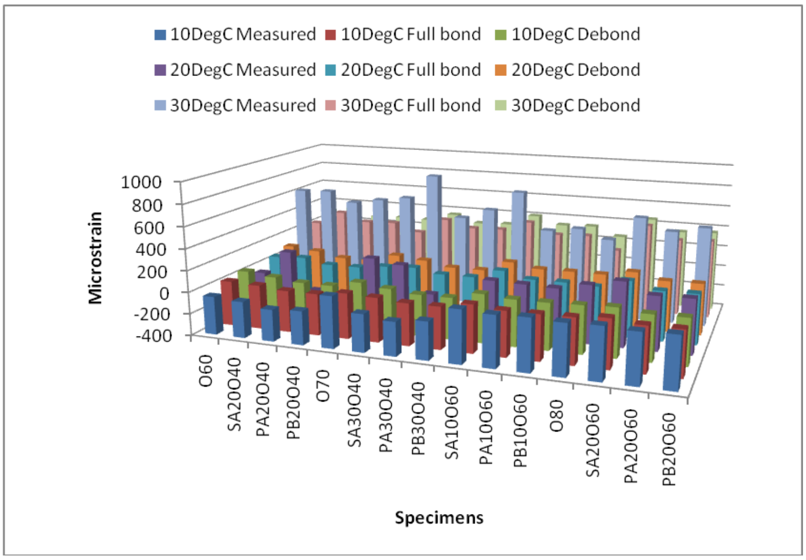


Fig. 9 Strain at 20 mm from the bottom of the overlay at 10 $^{o}$C, 20 $^{o}$C and 30 $^{o}$C (DegC)

*3) Stress*

The contour plots of the longitudinal stresses for the control specimen with 80 mm - thick overlay, 20 mm - sand asphalt and 60 mm - overlay, 20 mm - SAMIs A and B and 60 mm - overlay with the load placed at the centre directly above the crack tip as shown in Fig. 5 are shown in Figs. 10, 11, 12, and 13, respectively. It can be seen from the figures the potential of SAMIs to relieve stress in the overlay.

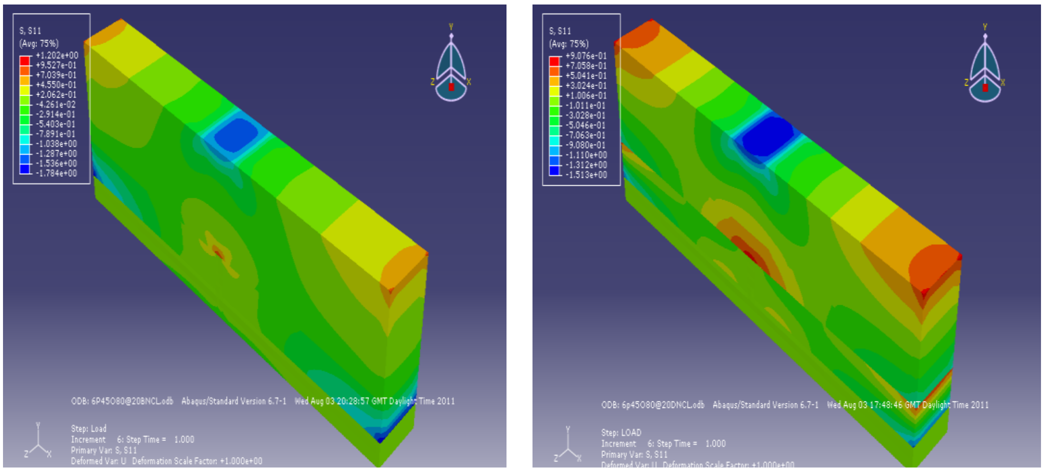

(a) (b)

Fig. 10 80 mm - overlay at 20 $^{o}$C with centre load (O80) (a) Full bond (b) Debond

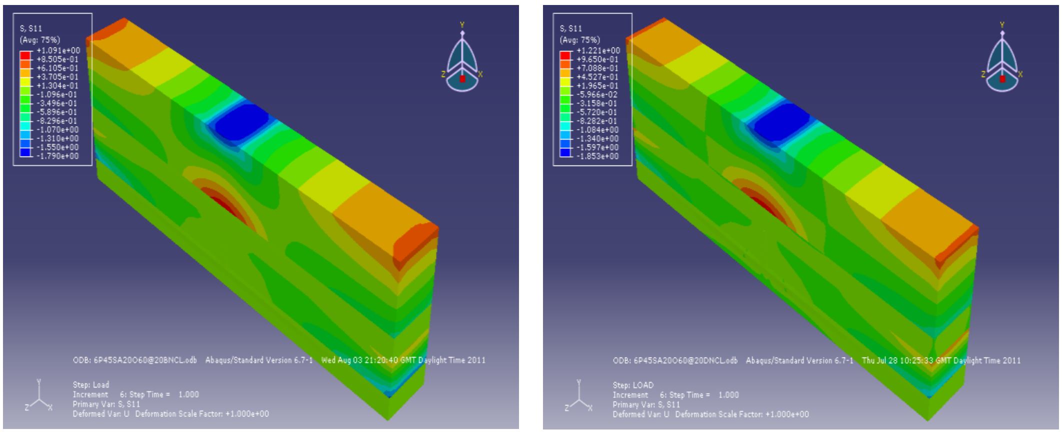

(a) (b)

Fig. 11 20 mm - sand asphalt with 60 mm - overlay at 20 $^{o}$C with centre load (SA20O60) (a) Full bond (b) Debond

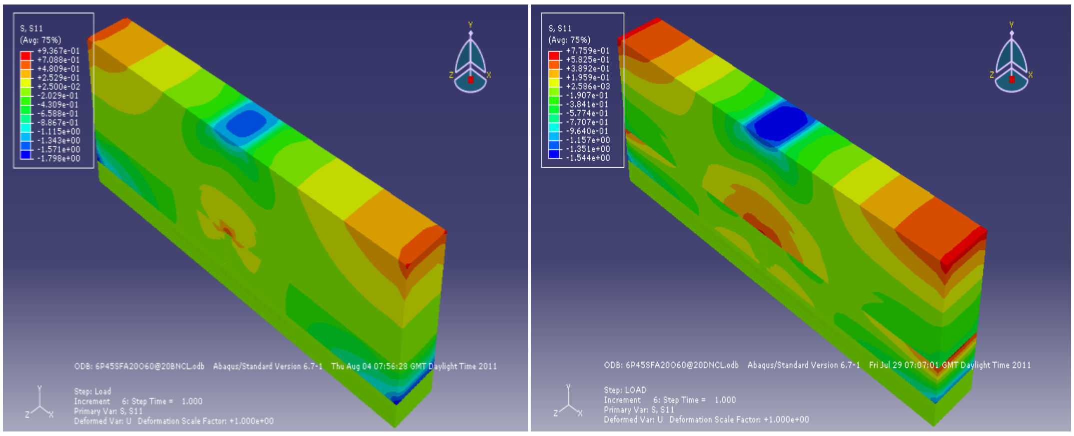

(a) (b)

Fig. 12 20 mm - proprietary SAMI A with 60 mm - overlay at 20 °C with centre load (PA20O60) (a) Full bond (b) Debond

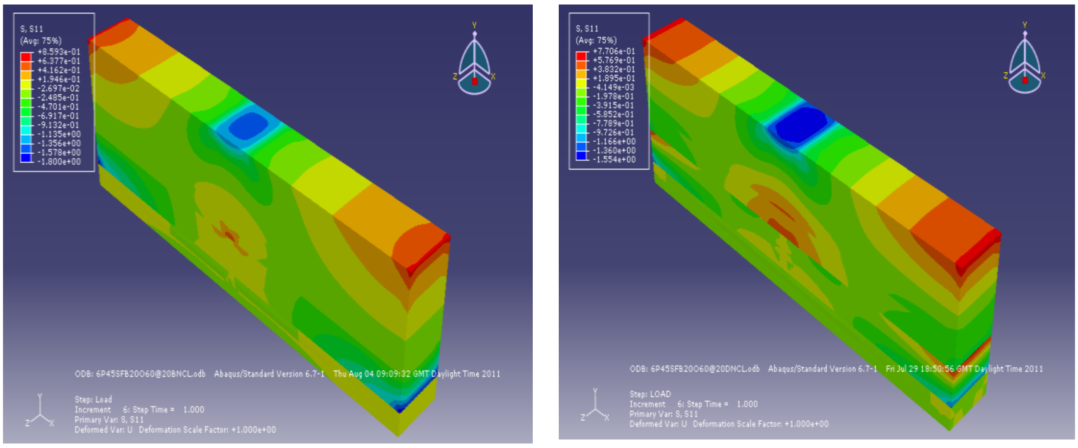

(a) (b)

Fig. 13 20 mm - proprietary SAMI B with 60 mm - overlay at 20 °C with centre load (PB20O60) (a) Full bond (b) Debond

Fig. 14 shows that when the load was placed at the centre, the predicted tensile stresses at 4 mm above the crack top in the specimens with SAMIs were smaller than the ones without SAMI. It can be seen that the stresses increased with increasing temperature. Also the figure shows that unlike all the other specimens, the specimens with sand asphalt as SAMI were in compression. This is because of the very low stiffness of the sand asphalt, which shows the pavement might be susceptible to permanent deformation. Fig. 15 shows that when the load was placed at the centre, the predicted tensile stresses at the bottom of the overlay of the specimens with proprietary SAMIs A and B were smaller than the predicted tensile stresses at the bottom of the overlay of their respective control specimens, while for the specimens with sand asphalt as SAMI, the predicted tensile stresses at the bottom of the overlay were greater than the ones for the specimens without SAMI. This agrees with the wheel tracking test which showed that the specimen with proprietary SAMIs A and B were able to retard reflective cracking [14]. This indicates both SAMIs are able to isolate the overlay from the stress/strain concentration at the crack tip, while the extreme low stiffness of sand asphalt inhibits its crack resistance ability. It is evident in this study that the SAMIs are able to reduce the tensile stress transferred to the overlay from stress concentration generated around the crack region by traffic loading.

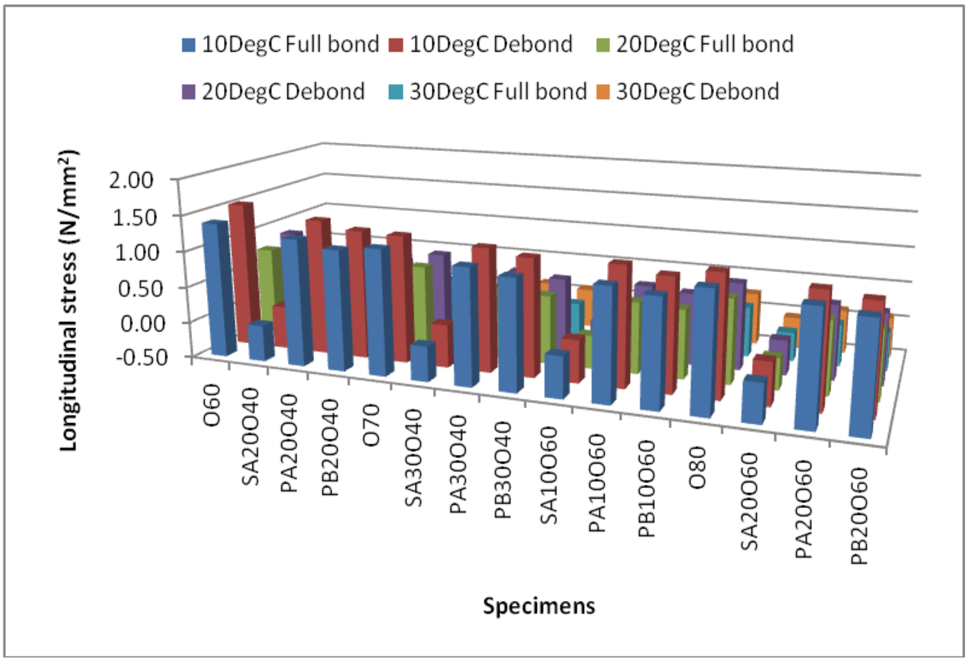


Fig. 14 Longitudinal stress at crack tip at 10 °C, 20 °C and 30 °C (DegC) with the load placed at the centre

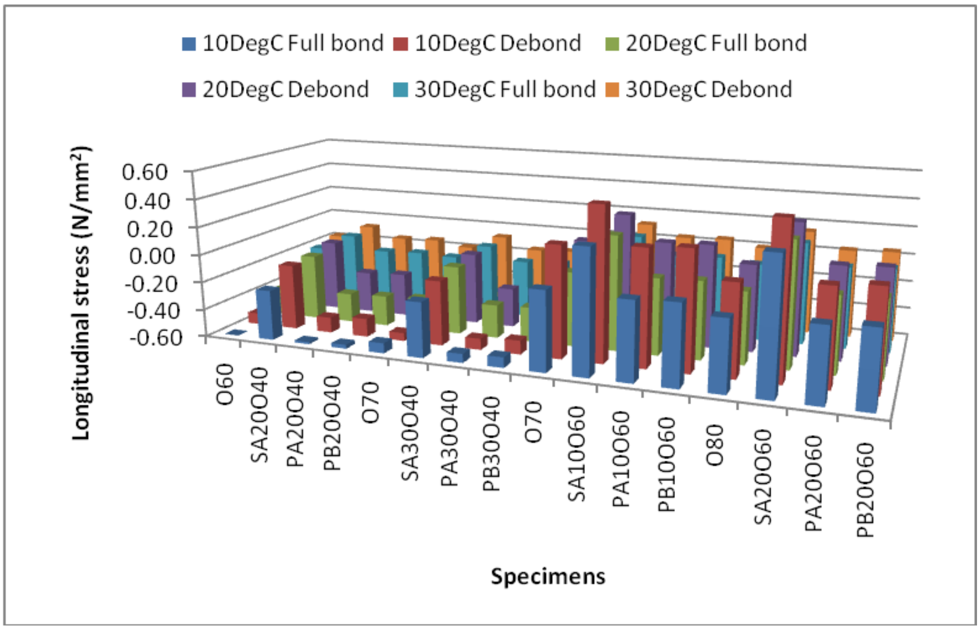


Fig. 15 Longitudinal stress at the bottom of overlay at 10 °C, 20 °C and 30 °C (DegC) with the load placed at the centre

## IV. CONCLUSIONS

Whilst the testing described in this study was clearly far from being a perfect simulation of a real pavement, it included the key feature of a rolling wheel and it is therefore believed that deductions are likely to be qualitatively valid. From this study, it was apparent that the closest match of the measured and predicted (finite element) displacement and strain occurred when it was assumed that the SAMI was debonded from the underlying material. The presence of debonding was not unexpected since the tensile stresses generated at the SAMI/lower asphalt interface on either side of the crack calculated, were large. The predictions for sand asphalt were found to have worst agreement with the measured values. It was found that there was no clear advantage in the use of a thick SAMI compared to a thin one. Generally, the study showed that when SAMIs were introduced in cracked pavements to retard reflective cracking, greater deflection of the pavement occurred. This is due to the reduced bending stiffness of the pavement which accompanied the introduction of SAMIs of lower stiffness than the stiffness of the overlay and the existing pavement. The study showed that greater deflections, stresses and strains were predicted in the specimens with debond (slip between the SAMI and the base layer), which implied less crack resistance of the SAMIs in this condition, but because crack propagation was not modelled, the effect of the slip on the SAMIs' performance could not be quantified.

REFERENCES


[1] Shalaby A. and Frechette L., "Reflective cracking on C-SHRP Long Term Pavement Performance Sites," Proceedings of 4th International RILEM Conference, Ottawa, Canada, 2000, pp. 241-250.

[2] Song H., Paulino G.H., and Buttlar G., "Simulation of Crack Propagation in Asphalt Concrete Using an Intrinsic Cohesive Zone Model," *Journal of Engineering Mechanics 2006*, vol. 132, no. 11, ASCE, pp. 1215-1223.

[3] Collop A.C., Thom N., and Sangiorgi C., "Assessment of Bond using the Leutner Shear Test," *Proceedings of the Institution of Civil Engineers Transport*, 156. 2003. pp. 211-217.

[4] Sangiorgi C., Collop A.C., and Thom N.H., "A Non-destructive Impulse Hammer for Evaluating the Bond between Asphalt Layers in a Road Pavement," 2003 International Symposium on Non-Destructive Testing in Civil Engineering, Berlin. Germany.

[5] Scarpas A. and de Bondt A.H., "Finite elements simulation of reflective cracking in asphaltic overlays," HERON 1996, vol. 41(1), ISSN 0045-7316.

[6] Kwon J., Tutumluer E., and Kim M., "Development of a mechanistic model for geosynthetic-reinforced flexible pavements," *Geosynthetics International 2005*, vol. 12(6), pp. 310-320.

[7] Kim J. and Buttlar W.G., "Analysis of Reflective Crack Control System Involving Reinforcing Grid over Base-Isolating Interlayer Mixture," *Journal of Transportation Engineering 2002*, pp. 375-384.

[8] Ozer H., Al-Qadi I.L., Wang H., and Leng Z., "Characterisation of interface bonding between hot-mix asphalt overlay and concrete pavements: modelling and *in-situ* response to accelerated loading," *International Journal of Pavement Engineering 2011*, DOI:10.1080/10298436.2011.596935.

[9] Sousa, J., Pais, J., Saim, R., Way, G., and Stubstad, R., "Development of a Mechanistic Overlay Design Method Based on Reflective Cracking Concepts," Final Report for Rubber Pavements Association, Consulpav International, 2001.

[10] Wu R.Z. and Harvey J.T., "Evaluation of Reflective Cracking Performance of Asphalt Mixes with Asphalt Rubber Binder using HVS Tests and Non-local Continuum Damage Mechanics," Proceedings of 6th International RILEM Conference, Chicago, U.S.A. 2008, pp. 3-12.

[11] Minhoto M.J.C, Pais J.C., and Pereira P.A.A., "Reflective Cracking Behaviour for Traffic and Temperature Effects," Proceedings of 6th International RILEM Conference, Chicago, U.S.A. 2008, pp. 551-561.

[12] Pais J.C. and Pereira P.A.A., "Predictions of Existing Reflective Cracking Potential of Flexible Pavements," Proceedings of 4th International RILEM Conference, Ontario, Canada, 2000, pp. 155-164.

[13] Abaqus Theory Manual. Abaqus Theory Manual, Dassault Systemes, U.S.A 2007.

[14] Ogundipe O.M., Mechanical Behaviour of Stress Absorbing Membrane Interlayers, Ph.D Thesis, University of Nottingham, Nottingham, United Kingdom. 2011.



**Olumide M. Ogundipe** obtained his first and second degrees in Civil Engineering at University of Ado-Ekiti, Nigeria (now Ekiti State University, Ado-Ekiti) and University of Ilorin, Kwara State, Nigeria, respectively. He bagged his Ph.D at the University of Nottingham, United Kingdom.

He is a Senior Lecturer in Civil Engineering Department, Faculty of Engineering, Ekiti State University Ado-Ekiti, Nigeria. His area of specialization is Highway and Transportation Engineering with special focus on Highway materials.

Dr Ogundipe is a member of the Nigerian Society of Engineers and he is registered to practise Civil Engineering by the Council for the Regulation of Engineering in Nigeria.